IEEE Access
Multidisciplinary | Rapid Review | Open Access Journal

Date of publication xxxx 00, 0000, date of current version xxxx 00, 0000

Digital Object Identifier 10.1109/ACCESS.2017.Doi Number

An online fade capacity estimation of lithium-ion battery using a new health indicator based only on a short period of the charging voltage profile

IGNACIO ALVAREZ-MONTESERIN[1], MIGUEL A. SANZ-BOBI[2]

[1]Enel Iberia SPA International Energy Company, Spain.

[2] Institute for Research and Technology (IIT), Comillas Pontifical University, Madrid, Spain.

Corresponding author: Ignacio Alvarez-Monteserin (jialvarezmonteserin@comillas.edu) and Miguel Sanz (masanz@comillas.edu)

ABSTRACT Currently, the most popular health indicator used to assess the degradation of lithium-ion batteries (LIBs) is the State of Health (SoH). This indicator is necessary to ensure the safety, degradation management, and good operation of the battery, for example, the correct estimate of the State of Charge (SoC). In this paper, a new health indicator is proposed as an alternative to the use of the SoH because it has a high correlation and similarity with the SoH and has the advantage that it can be calculated and/or estimated very easily. The new health indicator, named "Degradation Speed Ratio (DSR)" is calculated with variables directly measured (voltage and time), and it is not necessary to spend any time on the total charging cycle, therefore reducing waiting times about 84%. In addition, due to its high correlation with capacity, it is a significant marker of battery end-of-life (EoL). In this study, the obtained DSR and a Gaussian process regression (GPR) model were used to estimate the lost capacity and to compare it with existing models in the literature. The accuracy achieved using the DSR indicator as input is very high. Similarly, the results of a multilayer perceptron neural network (MLPNN) model are shown using the new indicator (DSR) as input to estimate the degradation. The sensitivity and precision of this NN model with unknown data are also very high.

INDEX TERMS Battery energy storage systems, data-driven estimation, degradation speed ratio, electric vehicles, lithium-ion batteries, model based estimation, state of health, battery energy storage systems.

I. INTRODUCTION

There are more and more devices using Lithium-ion cells in our lifestyle: laptops, electric vehicles (EV), Battery Energy Storage Systems (BESS) [1].

BESS are booming owing to climate change, the increase in renewable energy (e.g., wind farm, solar power plant, etc.), to provide stability to the electricity grids (micro-grid [2]), and the need for this kind of energy to store its surplus.

In the lithium-ion battery (LIB) market, different types of cells are manufactured, some of which are indicated to store energy (BESS), and others are used to make high-power energy systems, such as electric vehicles and sccotters. Therefore, each cell is unique owing to the manufacturing and battery chemistry.

In addition, there are different operating and environmental conditions (e.g., C-Rate, deep discharge, operating temperature, etc.). Therefore, the battery ageing process for Li-ion cells is different for each one, and knowing the battery aging is key to their operation to prevent failures. There is an attempt to solve this problem by implementing a precise State of Health (SoH) estimation method in the battery management system (BMS).

The SoH estimation is necessary for the correct operation of these batteries to determine the current energy storage and power supply in relation to the initial one for which it was designed.

Due to the relevance of having a good SoH estimation in order to know its health condition, in scientific literature several SoH methods can be found based on different

This article has been accepted for publication in a future issue of this journal, but has not been fully edited. Content may change prior to final publication. Citation information: DOI 10.1109/ACCESS.2022.3143107, IEEE Access

strategies and algorithms. Some of these are carried out through offline processes [3] [4], and others can be developed as online estimation methods [5] [6] [7].

The internal parameters of battery cells (e.g., impedance, internal resistance, etc.) are difficult to monitor by any BMS because of their difficult access during operation. However, the temperature, current, and voltage are external variables of the battery that can be directly measured, and their characteristics can be analyzed to use them in the battery aging process estimation. For this reason, the internal parameters of the LIB cannot be used in online processes to estimate the battery capacity.

Thus, in the literature, many different methods focus on estimating the SoH of batteries with increased precision. They can be classified into three categories:

(1) Direct measurements based on internal resistance measurement [3], the impedance measurement method [8], and the Coulomb counting method [9] are the most frequently applied.
(2) Model-based methods. They consider the battery as an electrochemical, electrical, or empirical model: e.g. equivalent circuit model (ECM) or electrochemical impedance model (EIM).
(3) Data-driven methods. They are based on features extraction approaches from observed values of variables able to be measured. They are flexible and use machine learning approaches.

Typically, data-driven methods use data from cell temperatures, currents, voltages, etc., obtained through several charging/discharging cycles. However, not all of these methods can extract data when the battery is in operation. Liu *et al.* [10] proposed a health indicator (HI) using data voltage ranges during charging and discharging processes.

Chen *et al.* [11] analyzed the constant current discharge voltage curve to describe the degradation of a battery, and they used a least-square-supported vector machine (LS-SVM) model to estimate the SoH.

Feng *et al.* [6] used a charging voltage profile interval of 15 min and a support vector machine (SVM) model. This model was trained using incremental capacity analysis (ICA) and open-circuit voltage (OCV) model-based data.

More complex methods have been proposed by He *et al.* [12] and Bien *et al.* [13], who obtained new features of interest (FOIs) through ICA, dQ/dV curves, and their voltage peaks. Finally, they estimated the SoH using a linear model.

Many papers have proposed HI, which have high correlations with the SoH [14], and are carried out through the characteristics of battery discharge [15][16]. These methods are difficult to implement in real-life applications because they are developed for optimal laboratory conditions, and these features only occur in constant-current discharges; the actual battery operation does not occur under these conditions.

Wang *et al.* [17] proposed a new HI based on a high correlation with the capacity; later on, this HI was estimated using an equivalent circuit model (ECM). A constant-voltage charging curve was used to estimate this HI, for which the battery must first reach the maximum voltage (4.2V).

Zhang *et al.* [18] extracted the charging times between two specific voltages to estimate the SoH through a Gaussian method: the GPR model. Thus, a comparison of some intervals of charging times between voltages is made, and even of the entire CC charging cycle (from the minimum to the maximum voltage), for which the method also requires reaching the maximum voltage of the battery to be estimated.

Tan *et al.* [19] proposed nine different FOIs based on CC charging curves and their gray relational coefficients vs. SoH. The best value was 0.98, but it required a full charge to reach this goal. Subsequently, the method applies a long short-term memory (LSTM) network to predict the SoH.

Meng *et al.* [20] used the charging voltage profile optimized by the NSGA-II algorithm to estimate the SoH. However, to do this, it is necessary to know the SoC for these voltages.

Tian *et al.* [21] proposed measuring the temperature differences in a specific voltage interval during constant charging using a support vector regression model to estimate the SoH. The results were compared with those obtained using the ICA method.

This paper proposes a new HI based on charging voltage profiles to solve some of the problems mentioned before and to cover some of the gaps detected in the state-of-the-art methods. In real-life applications, the battery charge, carried out under constant current, is always performed by the BMS under controlled conditions and, therefore, meets the convenient requirements to be measured to estimate the new HI described in this paper.

In addition, the proposed method does not require a complete charge/discharge cycle or a complete charge, not even when the battery is completely discharged at the beginning of the new charge cycle. This method is valid for all lithium-ion battery models and their different charging conditions due to the voltage range duration is measured with the same charging current.

Thus, battery operation can be performed according to the control signal. A constant charging current (for a short time period) is the only requirement for measuring time and voltage. Furthermore, this constant current can be supplied from the BMS for any short period during battery operation.

Therefore, the HI can be obtained at all times with a small interval of the charging voltage curve, e.g., in Electric Vehicles with the “braking” recharge. This new HI uses only one FOI; therefore, it is easier to implement, and its computational effort will be lower.

This paper is structured as follows: Section II presents the battery datasets used in this study and the CC charging curves. Section III includes an explanation of a novel battery health indicator, the correlations between this new HI and

This article has been accepted for publication in a future issue of this journal, but has not been fully edited. Content may change prior to final publication. Citation information: DOI 10.1109/ACCESS.2022.3143107, IEEE Access

capacity degradation, and the advantages of using this new HI. Section IV describes the validation of the proposed method using two datasets collected from different cells under different conditions, and the results are compared with those of the other methods. Finally, the conclusions are presented in Section V.

II. BATTERY DATASET AND DATA ANALYTICS

A. BATTERY DATASETS

Three datasets of LIBs were selected to analyze the behavior of the battery charging voltages and test the new HI proposed in this study. The first group from the NASA Ames Prognostics Center of Excellence are: B0005, B0006, and B0007 dataset battery [22]. Charging was carried out in a CC mode at 1.5A until the battery voltage reached 4,2V. Discharge was carried out at a CC level of 2A until the battery voltage fell to 2.7V, 2.5V and 2.2V for batteries 5, 6, and 7, respectively. The experiments were stopped when the batteries reached a 30% fade in rated capacity.

The second group from the Center for Advanced Life Cycle Engineering (CALCE) of the University of Maryland includes CS2-35, CS2-36, and CS2-37 [23]. In this case, charging was carried out in CC mode at 0.5A until the battery voltage reached 4,2V. Discharge was performed at a CC level of 1A, and the discharge cut-off voltage was 2.7V. The accelerated aging process was tested at an ambient temperature of 24 °C.

The last battery dataset from the Oxford University Research Archive (ORA) of the University of Oxford was BMP-cell2. For the profit-maximizing bucket model (BMP), the voltage limits were set to 3.42 V and 4.08 V, corresponding to 10 % and 90 % state of charge, and the charging current profile has variations from 2A until 17A.

B. VOLTAGE CURVE DATA ANALYTICS

The SoH is the most popular indicator reflecting the degradation of LIBs. The most widespread formula for this health indicator is shown in (1).

$$SoH\ (\%) = (C_{current}/C_{BOL}) \quad (1)$$

where $C_{current}$ and C_{BOL} are the current and BOL capacity, respectively. The value for BOL capacity, the first cycle of use, is 100%. In the same way, the value for the EOL is globally established at 20%, i.e., fade capacity is 80%.

Thus, the relationship between SoH and the fade capacity (FC) is:

$$Fade\ Capacity\ (\%) = 1 - SoH\ (\%) \quad (2)$$

In this study, a new HI is proposed based on observing the constant of certain characteristics of the current charging curves. The voltage curves for the different cycles are shown in Fig. 1.

Thus, it can be seen how, through the charging/discharging cycles (battery aging), the charging times needed to reach the target voltage (4.2 V generally) are reduced, i.e., they decrease throughout their life. Meanwhile, the battery degrades, and the SoH decreases. This behavior can be observed in all LIBs.

III. NEW PROPOSED BATTERY DEGRADATION INDICATOR

A. HEALTH INDICATOR DEFINITION

In this section, according to the analysis in the previous one, the development of a new degradation indicator shaped by data (voltages and times) from the CC charging voltage profile is exposed.

Thus, the aging features, only based on the voltage curve during the CC charging phase, were extracted.

As a result of the decrease in the charging times (due to battery aging), the slopes (calculated between any two points) of the charging voltage curves throughout the charging/discharging cycles also have variation, although it is increasing.

Thus, the slope for cycle 1 between points P1 and P2 is shown in Fig. 2 and is defined in (3).

$$m = (V_{4.1} - V_{4.0}) / (t_2 - t_1) \quad (3)$$

and for the cycle EOL in (4)

$$m' = (V_{4.1} - V_{4.0}) / (t'_2 - t'_1) \quad (4)$$

If the slopes of all the charging cycles (from cycle 1 to cycle EOL) of a battery are calculated between two voltage levels (for example, 3.8 V to 3.9 V), the trend is obtained as shown in Fig. 3.

The x-axis indicates the number of battery charging/discharging cycles and the y-axis shows the calculation of the slopes previously mentioned.

Thus, using these slopes a new proposed indicator called "degradation speed ratio" (DSR) is defined, which expresses the degradation speed of the battery measured in this voltage range [3.8-3.9V] throughout all its charging cycles (from cycle 1 to cycle EOL). V/s was used to measure the DSR. For the example shown in Fig. 3, this speed increases from 0.2 mV/s to 1.4 mV/s throughout the 168 charging cycles.

This indicator expresses for each voltage range (e.g. [3.8-3.9V]) what increase in the degradation speed (mV/s) a battery has, and the higher than speed, the greater the fade capacity is.

It is important to note that it is possible that the DSR slope decreases temporally in some of these calculations. This is due to the fact that the capacity at this moment increases. However, this effect is mitigated in successive charging cycles of the following DSR´s.

This article has been accepted for publication in a future issue of this journal, but has not been fully edited. Content may change prior to final publication. Citation information: DOI 10.1109/ACCESS.2022.3143107, IEEE Access

B. DEGRADATION SPEED RATIO. METHOD

Once the DSR has been defined and the first speed between two voltage points has been calculated (e.g. [3.8-3.9V]), the remainder can be calculated for successive intervals of the same charging voltage curve. Thus, e.g., the speeds for the NASA B0005 battery calculated in the intervals [3.8-3.9V], [3.9-4.0V], [4.0-4.1V], and [4.1-4.2V] are shown in Fig. 4.

After obtaining the speeds of the different voltage ranges, it is necessary to analyze the correlation between each DSR and the capacity indicator, 1-SoH (%) and 1/Cap (%), respectively.

In this study, the inverse of the capacity (%) and the fade capacity 1-SoH (%) were used because their correlation with the DSR can be better visualized, as can be observed in Fig. 5, that shows the four trends: two degradation rates [3.8-3.9V] and [3.9-4.0V], the capacity fade (%), and the inverse of capacity (1/Cap.(%)).

Fig. 6 shows the relationship observed between the SOH and DSR, and the possibility of using it when only one of these two variables is available in real time. In a very simplistic approach, based on a linear regression model, it is possible to conclude that the knowledge of DSR can provide a close idea of the SOH dynamic, even when it is not observed, and the similarity of both dynamics is within confidence bands at level of 95% in both cases.

These correlations must be calculated for the DSR ranges that need to be analyzed. Thus, Table I shows in the first four rows the correlation between the DSR Ranges [3.8-3.9V], [3.9-4.0V], [4.0-4.1V] and [4.1-4.2V] vs. 1 / Cap (%) and Fade Capacity (%) respectively.

The DSRs can be measured in whatever charging voltage range is deemed appropriate. In this study, DSR R1 [3.8-3.9V] was selected since it has the best correlation coefficient, as is shown in Table I.

To reduce the measurement times of the DSRs and have more DSR ranges available for the method, the best correlation range ([3.8-3.9V]) was split into four subranges, and their correlation coefficients were subsequently calculated. Thereby, if a cell in an instant does not need to charge in that voltage range, it will be performed in another chosen one. For example, DSR R8 is the first option and DSR R7 is the second option, [3.850-3.875] and [3.875-3.9], because they have the highest correlation coefficient.

In this study, four subranges were deepened, i.e., a voltage increase of 0.25V, but the voltage range can continue to be reduced according to needs and correlation analysis can be performed with the capacity variable to be corroborated.

Thus, the choice of the voltage range is made with the maximum correlation index because all data are available. However, in real life, when the entire dataset is not available, the choice of voltage range can be made according to several criteria due to the versatility of the indicator.

For example, it is possible to look at the charging profiles (observed during a week, e.g.,) when a battery begins its life (during its first charge cycle) and see which voltage ranges are the most used or have the highest frequency. Thus, it is possible to select (to estimate the battery fade capacity) one, two, three, or several of these voltage ranges. Hence, a real and optimal dataset will be built (to be used for this indicator) because a higher frequency of use area in battery operation will be covered.

In case of limited resources, a unique voltage range will be chosen, the one with the highest frequency of use. Once this range has been chosen, and due to the fact that the voltages and the time are always available, the DSR can be easily calculated.

Another example is the behavior of the DSR on the lithium-ion battery "BMP-cell2" working with different charging currents has also been analyzed, as shown in Fig. 7. This battery operation is carried out with different charge/discharge current levels, and it is possible to measure (as Fig. 7 shows) the DSR in a voltage range [3.75-3.8V] using different charging currents on the same "BMP-cell2."

C. ADVANTAGES OF USING DSR

The main motivation of this work, are the advantages of using the DSR indicator. They are multiple, but the most important is its efficiency, especially when considering its simplicity of calculation versus its relevance (sensitivity to capacity). Other remarkable advantages are listed below:

(1) DSR is an indicator with a high correlation coefficient of battery fade capacity since it relates and allows for not only the charging times ([17], [18]) but also charging voltage.

(2) The aforementioned time measurement reduction, e.g., a full charging/discharging cycle of the NASA B0005 battery spends approximately 7000 s (4000 charges + 3000 discharges). It is not needed to wait for the full charge and discharge battery cycle using this method, the time used to measure the predictive variables is reduced to 500 s, the time spent to calculate the DSR in the range [3.8-3.9V] in the BOL of the LIB. Therefore, it is obtained a reduction time in the measurement of 93% for the charging/discharge cycle and 84% with respect to the charging cycle.

This data of 500 s was used as a reference example in this paper, but these measurement times depend on the level of charging current used and the amplitude of the voltage range chosen (e.g.,0.1 V, 0.05V, 0.025V). The higher the intensity, the shorter the charging and measurement times used; similarly, the smaller the amplitude of the voltage range, the shorter the measurement time used.

(3) This new DSR indicator allows to see the trend of battery degradation at any time without having to estimate the SoH. If two DSRs are compared, in the same voltage range but measured at different times, it can be observed if this degradation remains constant over time (within confidence bounds) or if, by contrast, it is accelerating and how much, in order to

This article has been accepted for publication in a future issue of this journal, but has not been fully edited. Content may change prior to final publication. Citation information: DOI 10.1109/ACCESS.2022.3143107, IEEE Access

carry out any preventive operation or maintenance measures thereon.

(4) DSR can be measured in different voltage ranges, resulting in different DSRs that can advance the battery degradation process. For example, when will the battery reach its EOL, since as shown in Fig. 8, beginning with cycle 800, the fade capacity goes from being 25% to 100% in only 200 cycles, just like DSR, which goes from 0.07 mV/s to 0.81 mV/s in those 200 cycles.

(5) It can be used as an independent indicator and an alyternative option to substitute the traditional SoH, as explained later, since in real life, the SoH verification can only be carried out under laboratory conditions (capacity test), and this does not occur with the new DSR, which can be measured at any time.

(6) The implementation in a real BMS should be easy, because once the voltage range to be measured has been chosen, it is only necessary to calculate the slope of that piece of "voltage segment", and that is instantaneous.

D. DSR AS A HI

Keeping in mind the advantage number five mentioned above, for the validation of the DSR [3.875-3.9V] as an HI, the capacity estimation was performed with a single DSR range [3.875-3.9V] as input to a GPR model [24] for the six cells of the chosen datasets.

Table II illustrates the accuracy of the GRP model using DSR [3.875-3.9V] as input with the batteries B0005 and CS2_37.

Once the DSR indicator [3.875-3.9V] is certified as a valid instrument to evaluate battery degradation, it is possible to use a simple linear regression (LR) with the two previous DSR ranges: [3.825-3.850V] and [3.850- 3.875V] as model inputs to estimate the mentioned DSR [3.875-3.9V].

Table III shows the results obtained with the LR model [25]:

One of the advantages of using this DSR indicator [3.875-3.9V] is that the real measurement of the output variable can be obtained much more frequently and easily than the capacity, and thus be able to correct our model of real-time estimation.

As the output variable DSR [3.875-3.9V] has a very high SoH correlation ($R^2_{(AVR)} = 0.99$, for the six batteries in Table II), the DSR works as a very reliable estimator of the degradation capacity that can be measured in a more direct and simple way.

Although, in case of preferring the traditional indicator (the capacity as HI (SoH)), the data in Table II also show a high accuracy in the capacity estimation with a single input variable: DSR [3.875-3.9V].

There are other studies (e.g.[6] and [10]) that use a voltage segment to develop an HI, but on the one hand, e.g. Liu et al. [10] uses this "voltage segment" measured in a constant time interval (T), from a chosen voltage. Thus, this HI is a ΔV (voltage increase). In our method, the HI (DSR) considers voltage and time; therefore, the HI is sensitive to these two parameters. On the other hand, the Feng et al. [6] method needs "voltage segments" vs. SOC of the charging curve for different levels of SOHs and the Incremental Capacity Analysis (ICA), in order to train an SVM model. The online estimated SOH is calculated by comparing a "voltage segment" vs. SOC curve measured during 15 min, with the "voltage segment" curve calculated by the SVM model.

In our method, DSR only requires a small charging "voltage segment", which simplifies the method and makes it different from existing ones, because none (of the current methods proposed in scientific literature) uses the slopes calculated in a "voltage segment" of the charging curve profiles to analyze its variation and relationship with battery degradation.

IV. VALIDATION OF THE PROPOSED METHOD

Two different model methods were proposed to validate the DSR HI as a degradation indicator. First, the DSR indicator was used as an input variable of a GRP model [24] to estimate the degraded capacity and compare the results. This GPR model was used because it has been observed that the distribution of the data fits well with regions of Gaussian distribution.

Second, a similar experiment was performed using a neural network type multilayer perceptron with 8+4+2 layers. This will allow for modeling the possible non-linear characteristics underlying the relationships analyzed. Since, as is known, an MLPNN is a universal functional approximator able to model non-linear relationships with a good performance.

Later on, the behavior of this model was testing using an unknown dataset. Both of the approaches are described in the following subsections.

A. MODEL 1.GPR

In this sub-section, to test the new DSR indicator, it was used as an input of two GPR models to predict the SoH and to compare the proposed method with other studies.

In this way, the NASA battery dataset (cells B0005, B0006, and B0007) was used to train a GPR model in order to compare the results with studies that use the same datasets. Similarly, another GPR model trained with the CALCE dataset (cells CS2_35, CS2_36, and CS2_37) was developed for the same purpose to compare the results with similar models.

Once the models were trained, they were tested with values set aside (not used in the training process) for this purpose. Table IV lists the error indicators, and Fig. 9 shows the trends of the estimated and real values from the B0005 and CS2_35 batteries tested with each of their models.

Table V was created using the results of the models from the papers mentioned above in the state-of-the-art

This article has been accepted for publication in a future issue of this journal, but has not been fully edited. Content may change prior to final publication. Citation information: DOI 10.1109/ACCESS.2022.3143107, IEEE Access

introduction section to compare these results with the results obtained by the proposed method.

TABLE V

		[21]	[18]	[17]	[26]	This study		[10]	[27]		
B5	RMSE	0.0249	0.0077	0.0111	0.0084	**0.0106**	**0.0095**	0.015		RMSE	**CS2_35**
	MAE	0.049	0.0064	0.0088	0.0053	**0.0071**	**0.0065**			MAE	
	R^2	0.94		0.98	0.98	**0.99**	**0.99**			R^2	
B6	RMSE	0.0196	0.0163	0.0180	0.0180	**0.0186**	**0.0140**	0.017	0.0067	RMSE	**CS2_36**
	MAE	0.0597	0.0143	0.146	0.146	**0.0132**	**0.0079**			MAE	
	R^2	0.97		0.96	0.96	**0.98**	**0.99**			R^2	
B7	RMSE	0.0158		0.014		**0.0117**	**0.0107**	0.0124		RMSE	**CS2_37**
	MAE	0.0629		0.0098		**0.0095**	**0.0074**			MAE	
	R^2	0.96		0.97		**0.98**	**0.99**			R^2	

Furthermore, in order to analyze the DSR behavior using the GPR model to estimate the 1-SoH, for this study, another model has been trained using battery data sets B0005, B0006, B0007, CS2_35 and CS2_37, to be tested with the battery data set CS2_36, later on. In the same way, Fig. 10 shows the errors and the actual and estimated values trends.

The data used in the manuscript and in the papers cited in the "state of the art" of the introduction section are from a laboratory setting (NASA, CLACE, and OXFORD).

In real life, BMS systems implement integrated circuits (ICs) for the battery monitoring process to achieve errors below 0.25% of the voltage. Consequently, they will not contain any noise, and the GPR model will not be affected. Furthermore, sensor fault diagnosis models such as those proposed in [28] can be applied if necessary. Implementing both solutions, the measures used in the model in real life would not be compromised without corresponding detection.

The use of this new health indicator has another advantage: it depends only on the measurement of the voltage for its use; it is more robust against failures and greater ease of detection, not needing sensors of temperature, currents, resistors, etc., and other measures or calculations used as input in other prediction models.

B. MODEL 2.MLPNN

In addition, as an added value to this study, an MLPNN model was trained [29], which is the basic core of the major neural network designs used in deep learning. By using the new DSR indicator (DSR[3.825-3.850V], DSR[3.850-3.875V], and DSR[3.875-3.9V]) as the input of the basic core (MLPNN, 8+4+2 layers) of the neural network model, to estimate the battery degradation and analyze how it responds with other battery datasets not used in the training process model. Thus, the battery dataset used for training was formed by batteries B0005, B0006, CS2_35, and CS2_37, and later on, it was tested with B0007 and CS2_36 battery datasets.

The results are shown in Fig. 11 (test B0007 and test CS2_36) and Fig. 12 (test B0007+CS2_36), where good behavior with an unknown battery dataset can be seen as well as accuracy in the same order of magnitude as the models used in other studies, but with a “real” battery dataset.

As has been proved, in both models (GPR and MLPNN), the results are very good, tested with unknown data, validating the indicator proposed within the "research framework" defined in this paper.

Thus, the method and indicator provide speed in estimating the "fade capacity" and simplicity. It is expected that if more complex neural networks (deep learning) with this new indicator were used, the results would be even better, but that may be a motivation for future work.

V. CONCLUSIONS AND FUTURE RESEARCH WORK

In this paper, a new HI (DSR) of the degradation state of LIBs is presented, which is sensitive to aging and can even anticipate total failure (EOL). Both the sensitivity and accuracy are due to the fact that the DSR is calculated with the charging voltage and the charging times in determined voltage ranges (excluding the total charging/discharging process, temperatures, resistances, impedances, etc.), so the use of this DSR indicator is much faster to measure and estimate than traditional SoH.

In the same way, these two variables (voltage and time) can be measured directly during battery operation and very quickly, making it possible to determine the battery degradation level at all times (online), with the advantage that this entails for SoC calculating and battery maintenance. This makes it very easy to implement in any BMS system.

Using these two variables (voltage and time), the newly proposed DSR indicator can be calculated easily (no regression model is needed) and quickly (measuring these variables and performing two operations (subtraction and division). In addition, this new HI (DSR) can be obtained at any time during battery operation and being able to choose between any voltage range and different currents.

As has been shown, the DSR indicator has very accurate results when used as input models owing to its high sensitivity and similarity in the battery capacity evolution, which makes the computational effort, for model development, very low and makes high-accuracy prediction models.

In this paper, the empirical results of the developed models are presented and compared with other data-driven methods. In addition, the results of three GPR and MLPNN models trained with data from four batteries and validated with different battery datasets are presented. The results have high accuracy ($R^2 = 0.98$) for unknown data in both models.

Therefore, in conclusion, the method used can be replicated in other scenarios, since both the GPR and MLPNN models were tested with "real" unknown datasets. The authors consider that these tests suggest that the indicator and model can be replicated for any lithium-ion battery.

Future research work related to this study may focus on the development and implementation of this new method of evaluating battery degradation in a real BESS. Thus, the new indicator (DSR) can be evaluated and compared with a traditional SoH.

ACKNOWLEDGMENT

The authors would like to thank the CALCE Battery Research Group, University of Maryland, NASA for providing valuable battery degradation datasets and the Oxford University Research Archive (ORA) of the University of OXFORD.

REFERENCES

[1] N. Li, F. Gao, T. Hao, Z. Ma, and C. Zhang, "SOH Balancing Control Method for the MMC Battery Energy Storage System," *IEEE Trans. Ind. Electron.*, vol. 65, no. 8, pp. 6581–6591, 2018.

[2] D. Tran and A. M. Khambadkone, "Energy management for lifetime extension of energy storage system in micro-grid applications," *IEEE Trans. Smart Grid*, vol. 4, no. 3, pp. 1289–1296, 2013.

[3] H. G. Schweiger *et al.*, "Comparison of several methods for determining the internal resistance of lithium ion cells," *Sensors*, vol. 10, no. 6, pp. 5604–5625, 2010.

[4] L. Chen, Z. Lü, W. Lin, J. Li, and H. Pan, "A new state-of-health estimation method for lithium-ion batteries through the intrinsic relationship between ohmic internal resistance and capacity," *Measurement*, vol. 116, pp. 586–595, Feb. 2018.

[5] L. Wang, C. Pan, L. Liu, Y. Cheng, and X. Zhao, "On-board state of health estimation of LiFePO4 battery pack through differential voltage analysis," *Appl. Energy*, vol. 168, pp. 465–472, 2016.

[6] X. Feng *et al.*, "Online State-of-Health Estimation for Li-Ion Battery Using Partial Charging Segment Based on Support Vector Machine," *IEEE Trans. Veh. Technol.*, vol. 68, no. 9, pp. 8583–8592, 2019.

[7] C. Weng, Y. Cui, J. Sun, and H. Peng, "On-board state of health monitoring of lithium-ion batteries using incremental capacity analysis with support vector regression q," *J. Power Sources*, vol. 235, pp. 36–44, 2013.

[8] A. Guha and A. Patra, "State of Health Estimation of Lithium-Ion Batteries Using Capacity Fade and Internal Resistance Growth Models," *IEEE Trans. Transp. Electrif.*, 2017.

[9] K. Soon Ng, C.-S. Moo, Y.-P. Chen, and Y.-C. Hsieh, "Enhanced coulomb counting method for estimating state-of-charge and state-of-health of lithium-ion batteries," *Appl. Energy*, vol. 86, pp. 1506–1511, 2009.

[10] W. Liu, Y. Xu, and X. Feng, "A Hierarchical and Flexible Data-Driven Method for Online State-Of-Health Estimation of Li-ion Battery," *IEEE Trans. Veh. Technol.*, vol. 9545, no. c, 2020.

[11] Z. Chen, X. Xia, M. Sun, J. Shen, and R. Xiao, "State of health estimation of lithium-ion batteries based on fixed size LS-SVM," *2018 IEEE Veh. Power Propuls. Conf. VPPC 2018 - Proc.*, 2019.

[12] J. He, Z. Wei, X. Bian, and F. Yan, "State-of-Health Estimation of Lithium-Ion Batteries Using Incremental Capacity Analysis Based on Voltage-Capacity Model," *IEEE Trans. Transp. Electrif.*, vol. 6, no. 2, pp. 417–426, 2020.

[13] X. Bian, Z. Wei, J. He, and F. Yan, "A Novel Model-based Voltage Construction Method for Robust State-of-health Estimation of Lithium-ion Batteries," *IEEE Trans. Ind. Electron.*, vol. 0046, no. c, pp. 1–1, 2020.

[14] D. Liu, X. Yin, Y. Song, W. Liu, and Y. Peng, "An on-line state of health estimation of lithium-ion battery using unscented particle filter," *IEEE Access*, vol. 6, pp. 40990–41001, 2018.

[15] J. Li, L. Wang, C. Lyu, L. Zhang, and H. Wang, "Discharge capacity estimation for Li-ion batteries based on particle filter under multi-operating conditions," *Energy*, vol. 86, pp. 638–648, 2015.

[16] Z. Deng, X. Hu, X. Lin, L. Xu, Y. Che, and L. Hu, "General Discharge Voltage Information Enabled Health Evaluation for Lithium-Ion Batteries," *IEEE/ASME Trans. Mechatronics*, vol. 4435, no. 2019, pp. 1–1, 2020.

[17] Z. Wang, S. Zeng, J. Guo, and T. Qin, "State of health estimation of lithium-ion batteries based on the constant voltage charging curve," *Energy*, vol. 167, pp. 661–669, 2019.

[18] Y. Zhang and Z. Tian, "State of health of lithium ion battery estimation based on charging process," *Proc. 2019 IEEE 3rd Adv. Inf. Manag. Commun. Electron. Autom. Control Conf. IMCEC 2019*, no. Imcec, pp. 688–692, 2019.

[19] Y. Tan and G. Zhao, "Transfer Learning with Long Short - Term Memory Network for State - of - Health Prediction of Lithium - ion Batteries," *IEEE Trans. Ind. Electron.*, vol. 67, no. 10, pp. 8723–8731, 2020.

[20] J. Meng, L. Cai, D. I. Stroe, G. Luo, X. Sui, and R. Teodorescu, "Lithium-ion battery state-of-health estimation in electric vehicle using optimized partial charging voltage profiles," *Energy*, vol. 185, pp. 1054–1062, 2019.

[21] J. Tian, R. Xiong, and W. Shen, "State-of-Health Estimation Based on Differential Temperature for Lithium Ion Batteries," *IEEE Trans. Power Electron.*, vol. 35, no. 10, pp. 10363–10373, 2020.

[22] B. Saha and K. Goebel., "Battery Data Set," *NASA Ames Prognostics Data Repository.2007*. [Online]. Available: https://ti.arc.nasa.gov/tech/dash/groups/pcoe/prognostic-data-repository/#battery.

[23] Pecht M., "Battery Data Set. CALCE," *CALCE Battery Research Group, Maryland, MD, 2017*. [Online]. Available:

https://web.calce.umd.edu/batteries/data.htm.

[24] C. E. and C. K. I. W. Rasmussen, *Gaussian processes for machine learning.*, vol. 14, no. 2. 2006 Massachusetts Institute of Technology, 2006.

[25] P. D. Grünwald, "Linear Regression," in *The Minimum Description Length Principle*, MIT Press, 2007, pp. 335–368.

[26] Y. Li, S. Zhong, Q. Zhong, and K. Shi, "Lithium-ion battery state of health monitoring based on ensemble learning," *IEEE Access*, vol. 7, pp. 8754–8762, 2019.

[27] T. Bak and S. Lee, "Accurate estimation of battery SOH and RUL based on a progressive lstm with a time compensated entropy index," *Proc. Annu. Conf. Progn. Heal. Manag. Soc. PHM*, vol. 11, no. 1, pp. 1–10, 2019.

[28] Q. Yu, C. Wan, J. Li, R. Xiong, and Z. Chen, "A model-based sensor fault diagnosis scheme for batteries in electric vehicles," *Energies*, vol. 14, no. 4, 2021.

[29] J. M. Keller, D. Liu, and D. B. Fogel, "Multilayer Neural Networks and Backpropagation," in *Fundamentals of Computational Intelligence: Neural Networks, Fuzzy Systems, and Evolutionary Computation*, IEEE, 2016, pp. 35–60.

IGNACIO.ALVAREZ-MONTESERIN. received the B.S. degree in Electronic and Control Engineering and later on the M.S. degree in Industrial Engineering from the University of Salamanca, Spain in 2000. He is currently a member of the *Heat rate and BESS monitoring Center*, since 2018, of Enel SPA, International Energy Italian Company. He worked for 10 years in control systems and operation, developing energy efficiency and monitoring control systems. He is currently collaborating with the Technological Research Institute (IIT) through Miguel A Sanz, to develop this research in the lithium-ion batteries field, and pursuing the Ph.D. degree in Engineering Systems Modeling at the Engineering School of the Comillas Pontifical University, Madrid, Spain.

MIGUEL Á. SANZ-BOBI (Senior Member, IEEE) is currently a Professor with the Telematic and Computer Science Department, and also a Researcher with the Institute for Research and Technology (IIT), both within the Engineering School, Comillas Pontifical University, Madrid, Spain. He divides his time between teaching and research in the artificial intelligence field applied to diagnosis and maintenance of industrial processes. He has been the main researcher in more than 40 industrial projects over the last 25 years, related to the diagnosis in real time of industrial processes, incipient detection of anomalies based on models, knowledge acquisition and representation, and reliability and predictive maintenance. All these projects have been based on a combination of artificial intelligence, new information technologies, and data mining techniques.

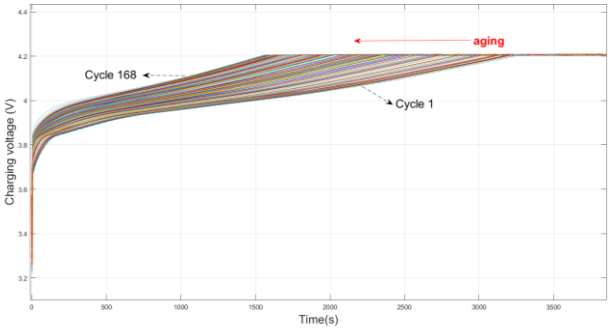

FIGURE 1. Charging voltage profiles from cycle 1 until cycle end of life.

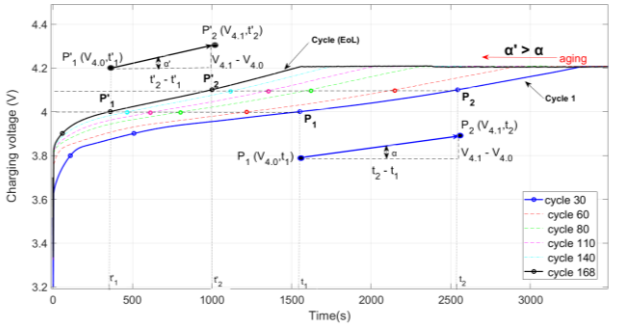

FIGURE 2. Slope variation calculation from cycle 1 (points P1 and P2) until cycle end of life points (P'1 and P'2).

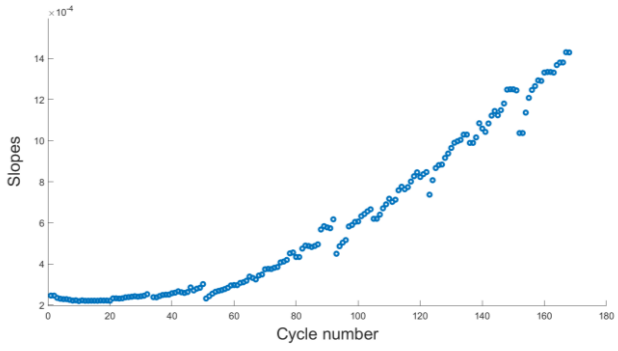

FIGURE 3. Voltage range measured [3.8-3.9 V] for NASA B0005 battery.

This article has been accepted for publication in a future issue of this journal, but has not been fully edited. Content may change prior to final publication. Citation information: DOI 10.1109/ACCESS.2022.3143107, IEEE Access

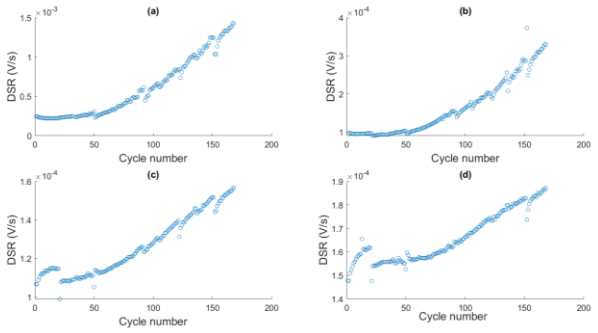

FIGURE 4. Degradation Speed Ratio for NASA B0005 battery. (a) DSR range [3.8-3.9 V]. (b) DSR range [3.9-4.0 V]. (c) DSR range [4.0-4.1 V]. (d) DSR range [4.1-4.2 V].

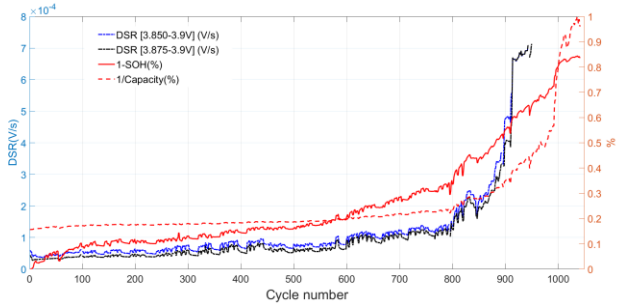

FIGURE 5. DSR [3.850-3.9 V] and DSR range [3.875-3.9 V] vs. 1-SOH and 1/Capacity.

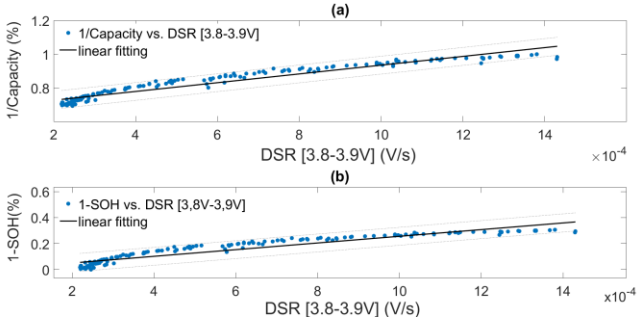

FIGURE 6. Relationship observed that exists between the SOH and the DSR. (a) 1/Capacity vs. DSR [3.8-3.9 V]. (b) 1-SOH vs. DSR [3.8-3.9 V].

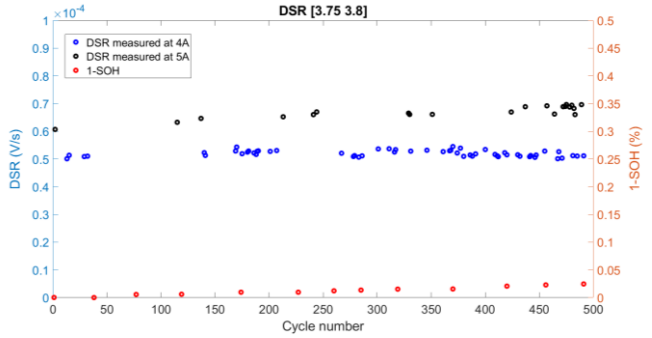

FIGURE 7. Degradation Speed Ratio for OXFORD BMP-Cell2 battery. DSR range [3.75-3.8 V] and 4A and 5A of current measure.

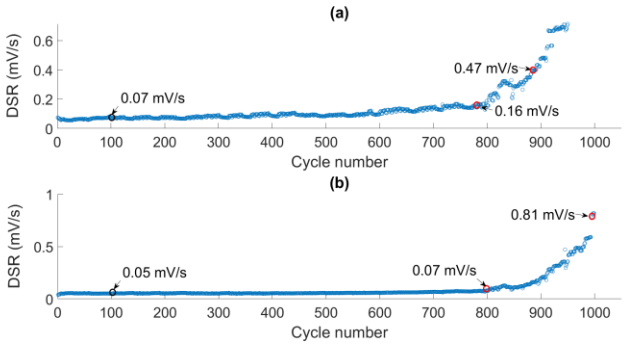

FIGURE 8. Degradation Speed Ratio for CALCE CS2_37 battery. (a) DSR range [3.8-3.9 V]. (b) DSR range [3.9-4.0 V].

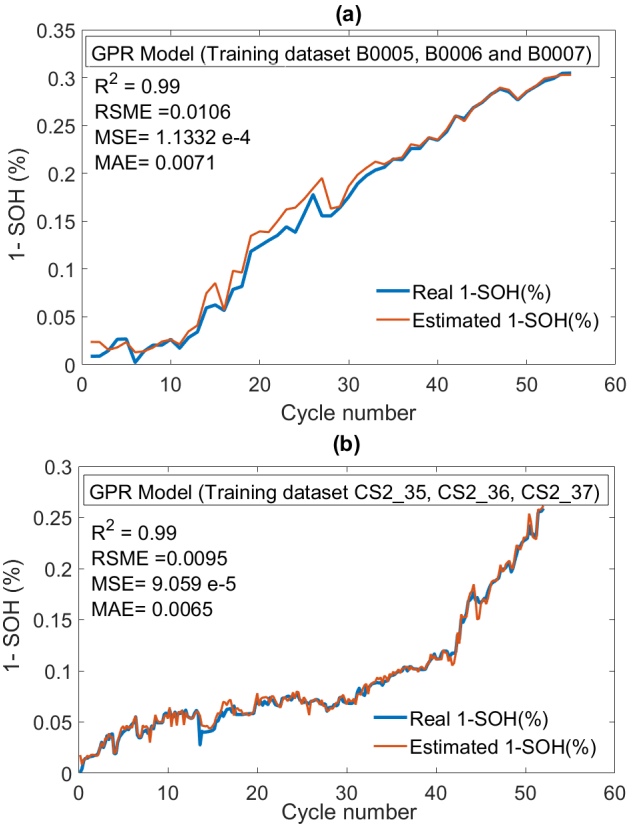

FIGURE 9. GPR model trend. (a) Tested with B0005 battery dataset. (b) Tested with CS2_35 battery dataset.

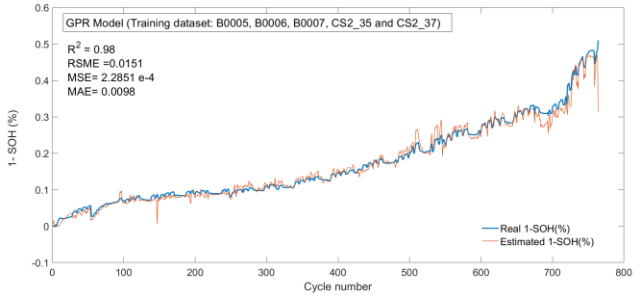

FIGURE 10. GPR model trend. Tested with CS2_36 battery dataset.

This article has been accepted for publication in a future issue of this journal, but has not been fully edited. Content may change prior to final publication. Citation information: DOI 10.1109/ACCESS.2022.3143107, IEEE Access

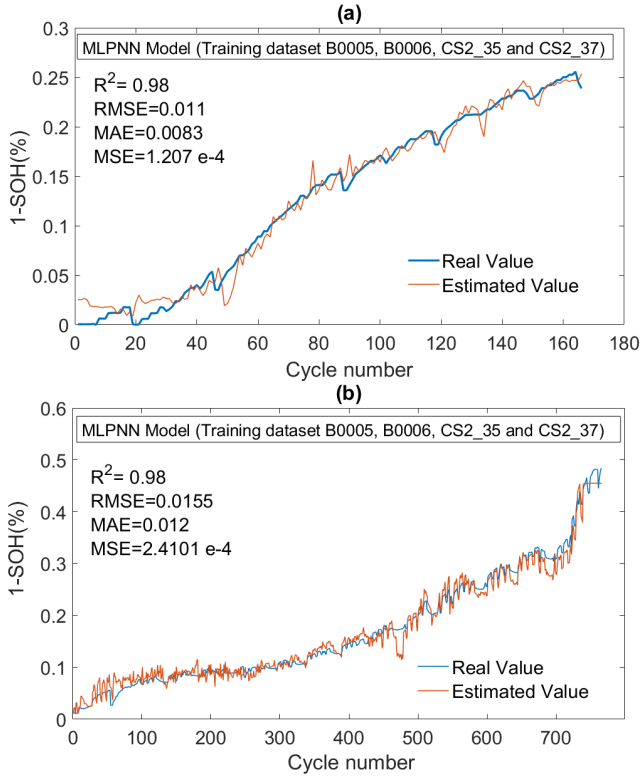

FIGURE 11. **MLPNN model trend. (a) Tested with B0007 battery dataset. (b) Tested with CS2_36 battery dataset.**

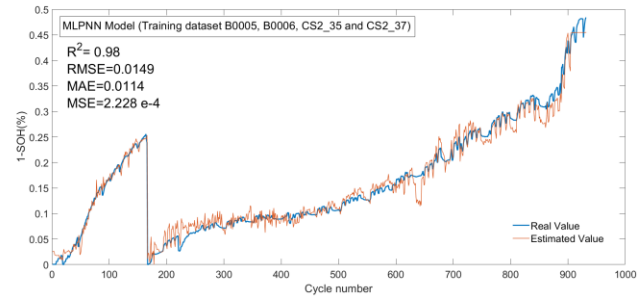

FIGURE 12. **MLPNN model trend tested with test B0007+CS2_36 batteries dataset.**

	DSR vs. 1/Cap (%)						DSR vs. Fade Capacity(%)					
	NASA Battery			CALCE Battery			NASA Battery			CALCE Battery		
	B0005	B0006	B0007	CS2_35	CS2_36	CS2_37	B0005	B0006	B0007	CS2_35	CS2_36	CS2_37
DSR R1 (3.8-3.9)	0.97	0.94	0.95	0.98	0.96	0.99	0.95	0.91	0.93	0.93	0.9	0.92
DSR R2 (3.9-4.0)	0.96	0.94	0.96	0.95	0.94	0,95	0.94	0.89	0.94	0.87	0.83	0.84
DSR R3 (4.0-4.1)	0.98	0.94	0.96	0.83	0.88	0,89	0.96	0.89	0.95	0.72	0.75	0.75
DSR R4 (4.1-4.2)	0.96	0.85	0.87	0.66	0.92	0,91	0.94	0.77	0.85	0.6	0.86	0.81
DSR R5 (3.8-3.825)	0.98	0.89	0.94	0.92	0.89	0.90	0.97	0.86	0.90	0.85	0.80	0.83
DSR R6 (3.825-3.85)	0.96	0.91	0.94	0.93	0.89	0.92	0.93	0.88	0.92	0.86	0.80	0.84
DSR R7 (3.85-3.875)	0.95	0.93	0.93	0.96	0.94	0.96	0.92	0.90	0.90	0.93	0.88	0.93
DSR R8 (3.875-3.9)	0.96	0.91	0.95	0.98	0.98	0.98	0.93	0.88	0.92	0.97	0.94	0.96
DSR R9 (ini-3.825)	0.97	0.91	0.90	0.92	0.73	0.90	0.95	0.88	0.85	0.89	0.62	0.84
DSR R10 (3.8-3.85)	0.97	0.93	0.94	0.92	0.89	0.92	0.95	0.90	0.92	0.86	0.80	0.85
DSR R11 (3.85-3.9)	0.96	0.92	0.94	0.98	0.97	0.98	0.93	0.89	0.91	0.96	0.93	0.96

TABLE I. **Correlation between the DSR Ranges [3.8-3.9V], [3.9-4.0V], [4.0-4.1V] and [4.1-4.2V] vs. 1 / Cap (%) and Fade Capacity (%) respectively.**

	DSR [3.875-3.9V] VS 1/Cap (%)					
	NASA Battery			CALCE Battery		
	B0005	B0006	B0007	CS2_35	CS2_36	CS2_37
RMSE	0.0063	0.0157	0.0097	0.0052	0.0050	0.0046
MAE	0.0041	0.0111	0.0072	0.0037	0.0034	0.0034
MSE	4.0297 e-5	0.00024	9.4209 e-5	2.7198 e-5	2.582 e-5	2.184 e-5
R^2	1	0.98	0.99	0.99	0.99	1

TABLE II. **GRP errors model using DSR [3.875-3.9V] as input vs. 1/Cap with NASA and CALCE batteries dataset.**

	input: DSR[3.825-3.850V] & DSR[3.850-3.875V] output: DSR[3.875-3.9V]					
	NASA Battery			CALCE Battery		
	B0005	B0006	B0007	CS2_35	CS2_36	CS2_37
RMSE	1.147 e-5	8.471 e-5	4.957 e-6	8.4766 e-6	7.968 e-6	7.351 e-6
MAE	7.537 e-6	4.595 e-5	3.774 e-6	6.731 e-6	6.355 e-6	5.109 e-6
MSE	1.316 e-10	7.176 e-9	2.458 e-11	7.185 e.11	6.348 e-11	5.404 e-11
R^2	1	0.98	1	0.98	0.98	0.99

TABLE III. **LR errors model using DSR [3.825-3.850V] and DSR [3.850-3.75V] as input vs. DSR [3.875-3.9V] with NASA and CALCE batteries dataset.**

	input: DSR[3.825-3.850V], DSR[3.850-3.875V] & DSR[3.875-3.9V]; output: 1-SOH (%)					
	GPR model (NASA Battery)			GPR model (CALCE Battery)		
	B0005	B0006	B0007	CS2_35	CS2_36	CS2_37
RMSE	0.0106	0.0186	0.0117	0.0095	0.0140	0.0107
MAE	0.0071	0.0132	0.0095	0.0065	0.0079	0.0074
MSE	1.1332 e-4	3.4537 e-4	1.3644 e-4	9.0595742 e-5	1.9589 e-4	1.1469 e-4
R^2	0.99	0.98	0.98	0.99	0.99	0.99

TABLE IV. **GPR errors model using DSR[3.825-3.850V], DSR[3.850-3.875V] and DSR[3.875-3.9V] as input vs. 1-SoH with NASA and CALCE batteries dataset.**

		[21]	[18]	[17]	[26]	This study	[10]	[27]		
B5	RMSE	0.0249	0.0077	0.0111	0.0084	**0.0106**	**0.0095**	0.015	RMSE	**CS2_35**
	MAE	0.049	0.0064	0.0088	0.0053	**0.0071**	**0.0065**		MAE	
	R^2	0.94		0.98	0.98	**0.99**	**0.99**		R^2	
B6	RMSE	0.0196	0.0163	0.0180	0.0180	**0.0186**	**0.0140**	0.017	0.0067 RMSE	**CS2_36**
	MAE	0.0597	0.0143	0.146	0.146	**0.0132**	**0.0079**		MAE	
	R^2	0.97		0.96	0.96	**0.98**	**0.99**		R^2	
B7	RMSE	0.0158		0.014		**0.0117**	**0.0107**	0.0124	RMSE	**CS2_37**
	MAE	0.0629		0.0098		**0.0095**	**0.0074**		MAE	
	R^2	0.96		0.97		**0.98**	**0.99**		R^2	

TABLE V. **Comparative results of this study and the state of the art.**